Biophysical Chemistry 147 (2010) 1–7

Contents lists available at ScienceDirect

Biophysical Chemistry

journal homepage: http://www.elsevier.com/locate/biophyschem

Unusual proximal heme pocket geometry in the deoxygenated *Thermobifida fusca*: A combined spectroscopic investigation

Alessandro Arcovito [a], Alessandra Bonamore [b], Jean Louis Hazemann [c], Alberto Boffi [b], Paola D'Angelo [d,*]

[a] Istituto di Biochimica e Biochimica Clinica, Università Cattolica del Sacro Cuore, Largo F. Vito 1, 00167 Roma, Italy
[b] Istituto Pasteur Fondazione Cenci Bolognetti, Department of Biochemical Sciences, University "La Sapienza", Rome, Italy
[c] Laboratoire Crystallographie CNRS, Grenoble, France
[d] Department of Chemistry, University "La Sapienza", Rome, Italy

ARTICLE INFO

Article history:
Received 16 October 2009
Received in revised form 25 November 2009
Accepted 25 November 2009
Available online 1 December 2009

Keywords:
XANES
EXAFS
Bacterial hemoglobin

ABSTRACT

The spectroscopic properties of the deoxygenated truncated hemoglobin from the actinobacterium *Thermobifida fusca* have been investigated by means of extended X-ray absorption fine structure (EXAFS), X-ray absorption near edge structure (XANES), and near infrared spectroscopies both at room and cryogenic temperatures. At room temperature the near infrared charge transfer band III occurs at 772 nm, a value that is unusually high for a canonical deoxygenated hemoglobin species, and can only be found as a transient species after photolysis in vertebrate hemoglobins and myoglobins or under strongly dehydrating conditions. EXAFS and XANES quantitative analyses, carried out in parallel with deoxygenated horse myoglobin, revealed an unusually short iron–histidine distance 1.90 ± 0.03 Å, significantly shorter than the deoxygenated horse myoglobin distance of 2.11 ± 0.02 Å. These findings provide novel structural basis for discussing the fine structural geometry of the proximal site, and eventually mapping the coordinates of the metal with respect to the pyrrole nitrogens and the proximal histidine nitrogen.

1. Introduction

The covalent link between the heme iron and the proximal histidine in hemoglobins is by far the most thoroughly investigated chemical bond in biochemistry. The atomic coordinates and electronic properties of the iron–histidine bond are considered as crucial parameters to adjust the reactivity of the heme-iron atom with the ligand in trans position. Thus, a strong bond with increased electron donation to the iron atom favors dioxygen cleavage (e.g. electron push effect in peroxidases), whereas a weaker bond is a prerequisite to preserve the integrity of the distal ligand in oxygen transport proteins. The stereochemistry of the iron–histidine bond is not only a major factor in determining the function of a hemeprotein, but is also the main conduit that governs the structural transitions at the basis of cooperativity in hemoglobins [1]. Exogeneous ligand binding to the sixth coordination position entails the displacement of the iron atom (about 0.5 Å) towards the heme plane with consequent shortening of the iron heme–pyrrole nitrogen bonds, and decreasing of the stretching frequency of the proximal iron–histidine bond. In hemoglobins, the proximal histidine follows the iron atom in its movement thus pulling the F helix in a rigid body displacement, that is subsequently transmitted to the helices that form the subunit interface [2]. Multiple spectroscopic investigations have focused on the fine structural and dynamic properties of the iron–histidine bond in order to assess the stereochemical details at the basis of the ligand binding process in hemoglobins and myoglobins.

In recent years, novel, unusual hemoglobin entities have further expanded the scope of the research [3]. In particular, the identification of novel "hemoglobin-like" proteins, widely distributed within prokaryotes and lower eukaryotes, widened the current understanding of hemoglobin functions and fostered a flourishing research on the properties of these unusual globins aimed at understanding their physiological function, their ligand binding properties, and their evolutionary relationships with respect to hemoglobins from higher eukaryotes. Within the bacterial hemoglobin superfamily, the so-called truncated hemoglobins represent a new frontier for hemoglobin research. These proteins are in fact characterized by a compacted globin fold (6 instead of 8 helices) and by an amazing variability of aminoacid side chains in the distal pocket in front of a proximal site characterized by the presence of a canonical proximal histidine [3,4]. In spite of extensive biochemical, biophysical and physiological studies, the hypotheses on the functional role of truncated hemoglobins are at present weak and rely on possible involvement in the scavenging of NO or oxygen radicalic species, within the framework of the cell response to oxidative or nitrosative stress [3]. Thus, biological investigations are presently running in parallel with physico-chemical characterizations of these novel globins in order to gain structural and functional insights into this amazing protein family.

* Corresponding author. Tel.: +39 06 49913751.
E-mail address: p.dangelo@caspur.it (P. D'Angelo).

0301-4622/$ – see front matter © 2009 Elsevier B.V. All rights reserved.
doi:10.1016/j.bpc.2009.11.006

Spectroscopic studies are based on the identification of structure sensitive signals (spectroscopic marker bands) that are related to the stereochemistry of the iron histidine bond. Near infrared absorption spectra are sensitive probes of the heme-iron electronic distribution and are strictly correlated to subtle rearrangement of the atomic frame around the critical Fe–His bond. In particular, the band III at about 760 nm has been assigned to a charge transfer band originating from a transition dipole moment involving electron donation from the porphyrin π^* to the Fe-d_z^2 orbital [5,6]. On the basis of this assignment, possible relationships between band III frequency and iron–heme plane distance have been worked out [7]. Nevertheless, near infrared spectroscopy does not allow a direct, quantitative estimate of the relevant atomic coordinates of the iron atom with respect to the heme plane or to the histidine nitrogen. Thus, direct, high resolution measurements of the iron stereochemistry by X-ray diffraction or absorption measurements are required in order to yield a complete picture of the functionally relevant structural rearrangements of the iron atom. In particular, X-ray absorption spectroscopy (XAS) is a powerful method for looking at the Fe-heme local structure [8]. Recent theoretical advances have made the extended X-ray absorption fine structure (EXAFS) analysis a primary, well established structural tool to investigate bond lengths at a precision of about 0.02 Å [9]. Moreover, a quantitative X-ray absorption near edge structure (XANES) analysis has been developed [10,11] and applied in combination with EXAFS to different system to extract information on bond distances and angular parameters. An accurate structural characterization has been obtained on metal ionic solutions [12], different heme models and heme containing proteins [13–15], showing that a combined analysis of the EXAFS and XANES regions of the spectrum is able to provide unambiguous details on the local structure in solution around the metal center.

In this framework, an investigation on the spectroscopic properties of the ferrous unliganded truncated hemoglobin from the actynomyces *Thermobifida fusca* (Tf-trHb) [16] has been undertaken with the aim of characterizing the fine structural properties of the Fe–histidine moiety as compared to ferrous unliganded horse myoglobin (h-Mb). The results of this study bring out relevant differences in the structure of the active site between Tf-trHb and h-Mb.

2. Experimental procedures

The hemoglobin from *T. fusca* was prepared and purified as described previously [16]. The protein was concentrated up to 1 mM heme with vivaspin PM10 concentrators (Sartorius Spa, Firenze). Protein concentration was determined by using an $\varepsilon = 182{,}000\ M^{-1}\ cm^{-1}$ at 421 nm for the CO derivative.

2.1. Near infrared absorption spectra

Near infrared spectra were carried out on a Jasco V570 spectrophotometer equipped with a PbS detector (Jasco Ltd., Japan). Low temperature spectra were measured in an Oxford liquid Nitrogen apparatus by diluting concentrated solutions of Tf-trHb in 50 mM phosphate buffer at pH 7.0 with glycerol (3:1 v/v glycerol/protein). A 100 mM solution of sodium dithionite buffered in 0.1 M phosphate buffer at pH 7.0 was then added to the degassed glycerol/protein solution to a final concentration of about 10 mM.

2.2. X-ray absorption measurements

Fe K-edge X-ray absorption spectra of h-Mb and Tf-trHb were collected in fluorescence mode at the BM30B beamline of the European Synchrotron Radiation Facility [17,18]. h-Mb was prepared by dissolving metmyoglobin in 1:5 glycerol–water solution buffered at pH 7 (70 mM phosphate) and adding 50 mM of sodium dithionite in nitrogen atmosphere. The final iron concentration was 6 mM. Tf-trHb was prepared by dissolving the protein in 1:5 glycerol–water solution buffered at pH 7 (80 mM phosphate) and adding 50 mM of sodium dithionite in nitrogen atmosphere. The final iron concentration was 4 mM. All the spectra were collected at 15 K. The storage ring was running in the two-third filling mode with a typical current of 170 mA. The monochromator was equipped with a Si (111) double crystal, in which the second crystal was elastically bent to a cylindrical cross section. The energy resolution at the Fe K-edge is 0.5 eV. The X-ray photon beam was vertically focused by a Ni–Pt mirror, and dynamically sagittally focused in the horizontal size. An array detector made by 30 Ge elements of very high purity was used. For each sample 10 spectra were recorded with a 7-s/point collection statistic and averaged. The spectra were calibrated by assigning the first inflection point of the Fe foil spectrum to 7111.2 eV.

2.3. EXAFS data analysis

The EXAFS data analysis has been performed using the GNXAS method [9,19], which is based on the theoretical calculation of the X-ray absorption fine structure signal and a subsequent refinement of the structural parameters. This theory allows the calculation of the interference signal in the cross section by solving the scattering of the photoelectron wave function in an effective muffin-tin potential. In the GNXAS approach, the interpretation of the experimental data is based on the decomposition of the $\chi(k)$ signal into a summation over n-body distribution functions $\gamma^{(n)}$ calculated by means of the multiple-scattering (MS) theory.

Previous investigations have shown that for a quantitative EXAFS analysis of hemeproteins MS four-body terms have to be accounted for [13–16,20]. The inclusion of these higher order contributions is essential to obtain a good agreement between theoretical and experimental data. The analysis of the two proteins has been carried out starting from the crystallographic coordinates of deoxy myoglobin at 1.15 Å resolution, up to a distance cutoff of 5 Å (PDB code=1A6N). The two-, three-, and four-body configurations in each cluster were grouped with a distance tolerance of 0.05 Å. Phase shifts were calculated using the standard muffin-tin approximation. A model EXAFS spectrum was generated by adding all the relevant single- and multiple-scattering contributions, and it was refined against the experimental data by using a least-square minimization procedure in which structural and nonstructural parameters were allowed to float. The quality of the fits was determined by the goodness-of-the-fit parameter R [9], and by careful inspection of the EXAFS residuals and their Fourier transforms (FT). A thorough description of the data analysis procedure and all the relevant parameters used in the minimization is given in Ref. [13].

2.4. Quantitative XANES analysis

The XANES calculations have been performed using the MXAN software procedure [8,10]. The analysis of the XANES spectra has been carried out using a cluster of thirty-one atoms, i.e., the porphyrin macrocycle, the histidine imidazole, and the oxygen of an unbound water molecule. The molecular potential for the nearest atoms, i.e., the FeN_5 cluster, was obtained using the spin-unpolarized, self-consistent field method imposing the formal valence of each atom. The exchange correlation part of the potential was determined by the X-α approximation. Inelastic processes were taken into account by a convolution with a phenomenological, energy-dependent, broadening function. All details of this kind of calculation are described in Ref. [22]. A constant experimental error corresponding to a noise-to-signal ratio of 0.012 normalized units (i.e. units for which the absorption jump is equal to 1) was chosen. The minimization of the χ^2 function was performed in the space of the n selected structural parameters (χ^2/n values are reported in the Results section to quantify the goodness of the fits). They are the core size, the Fe-heme displacement,

and distance of the Fe atom from the proximal histidine nitrogen N_h. During the minimization procedure, the outer atoms of the histidine and pyrrolic rings rigidly followed the motion of the N_h and nitrogen atoms of the porphyrin ring (N_p).

XANES difference spectra Tf-trHb–h-Mb were calculated starting from the 1A6N PDB structure taken as reference, by modifying the MXAN program as already done in a previous study [21]. Fitting difference spectra has the important advantage that some systematic errors of the XANES theory, mostly pertaining the photoelectron scattering on the heme plane, can be reduced. As the majority of the signal in solution is due to heme plane scattering, these errors affect the determination of axial parameters and render them, in solution, less accurate than what is reported for the myoglobin $P2_1$ crystals [22], where the heme plane and heme normal scattering can be experimentally decoupled. In the present case, it is reasonable that theoretical systematic errors associated to the heme plane scattering signals for h-Mb and Tf-trHb are very similar, so that they are partially eliminated in the difference spectrum. Accordingly, the present analysis of the XANES difference spectrum is less sensitive to the heme plane parameters (e.g. the Fe–N_p distance), but it is more accurate and more sensitive to the heme normal parameters (e.g. the Fe–N_h distance) as compared to the analysis of absolute XANES absorption spectra.

3. Results

3.1. Near infrared spectra

In order to unveil the fine electronic properties of Tf-trHb we have carried out a direct comparison of the near infrared absorption spectra of this protein with the canonical h-Mb. The Tf-trHb spectra have been acquired both at room (Fig. 1, panel A, at 293 K) and low temperature (Fig. 1, panel B, at 77 K) revealing the presence of an unusually strong and red shifted band III with respect to h-Mb. In fact, comparison of the spectra of Tf-trHb (Fig. 1, solid line) and h-Mb (dashed line) points out that the Tf-trHb displays a high-intensity band III peaked at 772 nm, 12 nm higher than that observed in h-Mb. Low temperature spectra confirm this large difference between the absorption peaks of the two proteins The presence of an unusually red shifted band III can stem either from a different electronic properties of the heme pocket or from a unusual geometry of the metal site. To shed light on the origin of this experimental evidence we acquired EXAFS and XANES spectra of Tf-trHb which were able to provide an accurate and independent determination of the local structure of the heme site.

3.2. X-ray absorption spectra

A quantitative estimate of the iron coordination geometry parameters can be obtained from the comparative analysis of the X-ray absorption spectra of Tf-trHb and h-Mb. In Fig. 2, the experimental XANES spectra (upper panel) and Fourier Transformed EXAFS spectra (lower panel) of the two samples are superimposed (dotted line h-Mb and solid line Tf-trHb). Looking at the XANES, the main difference between the two spectra is the blue shift of the rising edge of Tf-trHb as compared to h-Mb. Moreover, the absorption cross section of Tf-trHb increases at about 7150 eV and decreases at about 7170 eV, as evident from the [Tf-trHb–h-Mb] difference spectrum reported in the same panel of Fig. 2 (solid gray line). The blue shift of the rising edge can be

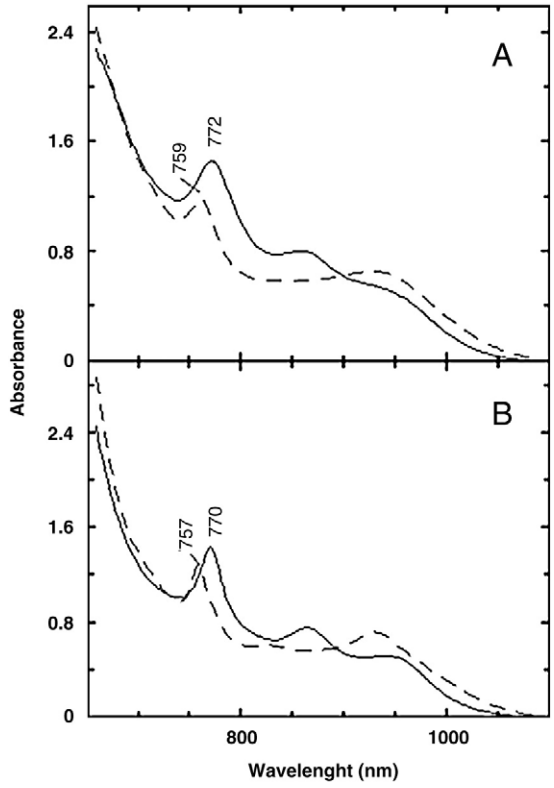

Fig. 1. IR spectra. Near infrared absorption spectra of deoxygenated Tf-trHb (solid line) in comparison with h-Mb (dashed line). Spectra were measured at 293 K (panel A) and 77 K (panel B) in 3:1 glycerol/buffer mixtures. Protein concentration was 1.1 mM heme, buffer was 50 mM phosphate at pH 7.0 in the presence of 20 mM sodium dithionite.

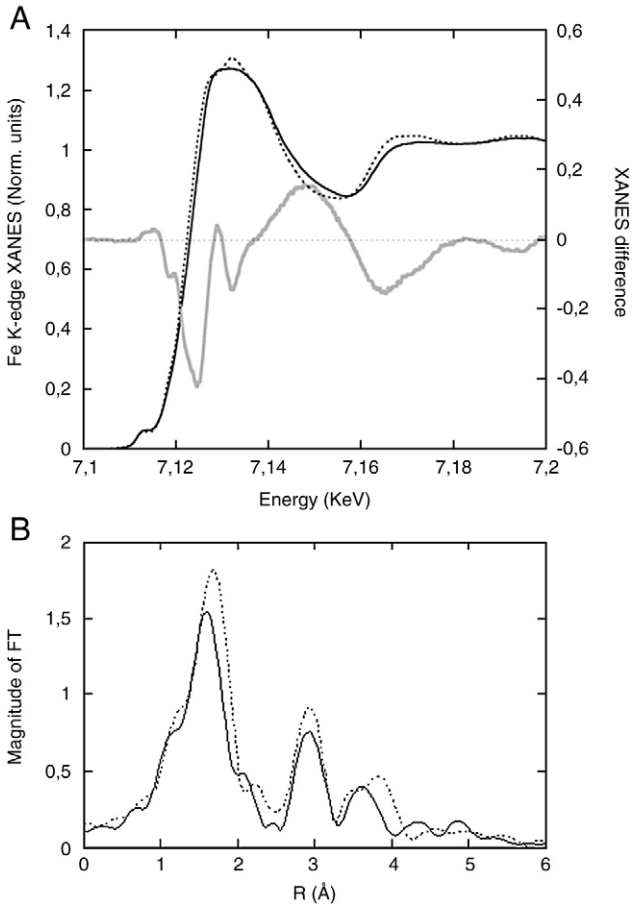

Fig. 2. XAS spectra. Upper panel: XANES spectra of h-Mb (dotted line) and Tf-trHb (solid line), and [Tf-trHb -h-Mb] difference spectrum (gray solid line). Lower panel: Comparison between their Fourier Transform of the experimental EXAFS spectra for h-Mb (dotted line) and Tf-trHb (solid line).

due to different mechanisms: 1) an increase of the iron redox state, which enhances the energy necessary to extract an electron from the metal [23]; 2) the binding of a sixth ligand in the case of a five-coordinate Fe-heme [22,24]; and 3) a decrease of the first-shell average distance [25]. Both 2 and 3 mechanisms act by changing the ligand field on the metal, and by increasing the energy of the empty electron states with p-symmetry. The UV/Vis spectrum of Tf-trHb (acquired on the same sample exposed to the X-ray beam, data not shown) closely resembles the h-Mb form, thus indicating that a negligible percentage, if any, of oxidized or bound Fe-heme is present. Note that both proteins have been measured in the presence of an excess of sodium dithionite (see Experimental procedures section), and it is well known that prolonged X-ray exposure determines a reduction of the iron heme disfavoring the contamination of oxidized species [11,15]. Therefore, the observed XANES changes are due to a decrease of the first-shell average distance. The h-Mb and Tf-trHb FT moduli of the EXAFS spectra extracted with a three-segmented cubic spline, have been calculated in the interval $k = 3.2–14.0$ Å^{-1} with no phase-shift correction applied. In both cases, the high-intensity peak at about 1.5 Å is associated with the first coordination shell around the iron atom. It comprises the four nitrogen atoms of the porphyrin ring, and one nitrogen atom of the proximal histidine. The second set of peaks, in the distance range between 2 and 3.5 Å contains all of the single and multiple-scattering contributions associated with the carbon atoms in the second coordination shell of both the porphyrin plane and the proximal histidine. The third set of peaks beyond 3.5 Å is mainly due to the single- and multiple-scattering contributions associated with the third shell of the tetrapyrrole macrocycle atoms. Simple inspection of the Fourier Transformed (FT) spectra offers interesting insight into the structural changes between h-Mb and Tf-trHb. It can be noticed that the first peak of Tf-trHb shows a lower intensity and shorter distance position as compared to h-Mb. This result is in agreement with the blue shift of the XANES edges and suggests a contraction of the first-shell average distance in Tf-trHb as compared to h-Mb.

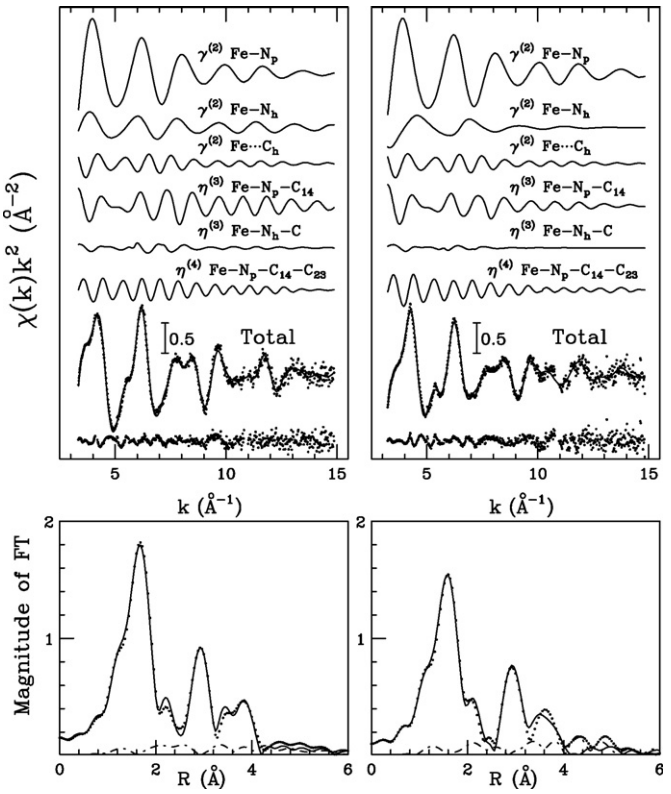

Fig. 3. EXAFS analysis. Fit of the h-Mb and Tf-trHb EXAFS spectra (left and right upper panels, respectively). From the top to the bottom of each panel, the following curves are reported: the Fe–N_p, Fe–N_h and Fe–C_h first-shell single-scattering signals, the Fe–N_p–C_{14} total three-body signals, and the Fe–N_p–C_{14}–C_{23} total four-body signals. The total theoretical signals (solid lines) are compared with the experimental spectra (dotted lines) and the residual curve. The lower panels show the nonphase-shift-corrected Fourier transforms of the experimental data (dotted line), of the total theoretical signal (solid line), and of the residual curves (dashed-dotted line).

3.3. EXAFS results

A quantitative estimate of the distances of the iron atom from the pyrrolic and histidine nitrogen atoms can be obtained from the analysis of the EXAFS data by means of the GNXAS program [7,19]. The results of the fitting procedure applied to h-Mb EXAFS data are shown in the left panel of Fig. 3. The spectrum is dominated by the first-shell two-body signals associated with the four nitrogen atoms from the porphyrin ($\gamma^{(2)}$ Fe–N_p) and the axial nitrogen atom from the histidine ($\gamma^{(2)}$ Fe–N_h). The latter contribution was treated as a separate single-scattering signal as the Fe–N_h bond length is about 0.07 Å longer than the average Fe–N_p bond length, according to the crystallographic values (PDB code=1A6N, see Table 1). In addition to the first-shell contributions, the simulation requires four carbon atoms at about 3.4 Å derived from the connecting methylene groups ($\gamma^{(2)}$ Fe–C_h). A good fit of the experimental data required the inclusion of the Fe–N_p–C_{14} three-body ($\gamma^{(3)}$) and the Fe–N_p–C_{14}–C_{23} four-body ($\eta^{(4)}$) total contributions. The dominant MS contribution is the Fe–N_p–C_{14} three-body pathway from the porphyrin, whereas the amplitude of the MS terms associated with the histidine is negligible owing to the low multiplicity. The theoretical signal closely matches the experimental data and the structural parameters obtained from the minimization are all in excellent agreement with the crystallographic values within the reported errors (Table 1).

The EXAFS data analysis of Tf-trHb has been carried out along the line of that of h-Mb. The minimization procedure has been carried out starting from the 1A6N structure of h-Mb and allowing distances and angles to float within a preset range of ±0.3 Å and ±5°, respectively. The experimental oscillations of the two samples show marked differences in the range between 7 and 12 Å^{-1}. Inspection of the theoretical signals shows that these differences originate from the modification in frequency and phase of the two-body $\gamma^{(2)}$ Fe–N_h signals. As a consequence different first-shell distances have been obtained from the fitting procedure, with a factor index value $R = 1.009 \times 10^{-5}$. In particular, whereas the Fe–N_p distance does not change in an appreciable way, a decrease of the Fe–N_h of 0.21 Å has been observed in going from the h-Mb to Tf-trHb (see Tables 1 and 2). Therefore, the contraction of the Fe–N_h distance is responsible for both the blue shift of edge and the shift of the FT first peak previously described. The Debye–Waller factors obtained for h-Mb and Tf-trHb from the fitting procedures are quite small and very similar between the two proteins. This suggests that in both cases the iron atom is involved in quite stiff bonds with the pyrrole and histidine nitrogens.

Table 1
h-Mb structural parameters. Structural parameters derived from the EXAFS analysis and from XRD data for h-Mb. Statistical errors are reported in parenthesis.

	Range of crystallographic distances (Å)[a]	EXAFS distance (Å)	EXAFS bond variance (Å^2)
Fe–Np	2.04−2.11	2.06 (1)	0.005
Fe–Ch	3.36−3.46	3.44(2)	0.004
C14−C23	1.42−1.48	1.39 (1)	0.011
Fe–Nh	2.14	2.11(2)	0.007

[a] Vojtechovsky, J.; Berendsen, J.; Chu, K.; Schlichting, I.; Sweet, R. M. *Biophys. J.* 1999, *77*, 2153-2174. PDB code: 1A6N.

Table 2
Tf-trHb structural parameters. Structural parameters derived from the EXAFS and XANES analysis for Tf-trHb. Statistical errors are reported in parenthesis.

	EXAFS distance (Å)	EXAFS bond variance (Å^2)	XANES distance (Å)
Fe–Np	2.05(1)	0.006	2.07(3)
Fe–Ch	3.43(1)	0.004	–
C14–C23	1.34 (1)	0.012	–
Fe–Nh	1.90 (2)	0.008	1.93(3)

3.4. XANES results

To further validate the EXAFS results we have performed a comparative analysis of the XANES difference spectrum [Tf-trHb–h-Mb], up to about 180 eV above the edge via the MXAN package [10]. The best fit (see Fig. 4) is obtained for a Fe–N_h distance to 1.93 ± 0.03 Å, while the Fe–N_p distance remains essentially equal to the starting value of 2.07 ± 0.02 Å, in perfect agreement with the EXAFS results reported in Table 2. The quality of the fit is satisfactory ($\chi^2/n = 1.74$), thus showing that the structural results obtained from the EXAFS analysis are compatible with the XANES data. It is worthwhile to note that the XANES and EXAFS analyses are independent, thus the convergence of the results strongly supports the reliability of the obtained local structure of the heme site.

4. Discussion

The near infrared data shown in Fig. 1 exhibit an unusually red shifted band III in Tf-trHb with respect to h-Mb both at 293 and 77 K. The 760 nm band, present in five-coordinate ferrous heme derivatives, has been assigned to a plane polarized charge transfer transition from the porphyrin π system to the iron d_{xy} orbital [3] or, alternatively, to an iron $d_x2_y2 \rightarrow e_g(\pi)$ orbital promotion [4]. In fact, in h-Mb the 760 nm band was shown to be sensitive to the local structure of the heme within the heme pocket, and in particular to the position of the iron with respect to the heme plane [5,27,28]. In both cases, the structural rearrangements leading to changes in the energy of the iron d orbitals, or the porphyrin π orbital system will affect the energy of the observed transition. The present data provide a clear picture of the structural properties of the iron-proximal histidine bond in the deoxygenated derivative of a truncated hemoglobin, and unambiguously show that the proximal site is widely different from that of typical vertebrate hemoglobins and myoglobins. It is interesting to consider the unusual band III position in Tf-trHb in the light of the dynamic behavior observed upon laser photolysis in vertebrate hemoglobins. The band III in deoxygenated vertebrate hemoglobins and myoglobins occurs at 760 nm and transiently shifts to about 770 nm in the nanosecond photoproducts of the CO bound derivatives [27]. The observed shift has been taken as a probe for the presence of a relaxed state in which the transiently generated penta-coordinate heme-iron resides in a position that is close to that typical of the hexa-coordinated, ligand bound species. In hemoglobins the nanosecond photoproducts then evolve towards the strained "unrelaxed" state typical of the "Tense" conformation that is represented, at equilibrium, by the canonical 760 nm band. The photoproduct relaxation, as monitored by near infrared, is thus considered as the most significant structural rearrangement that is functionally relevant to the mechanism of cooperativity. These considerations can be merged with recent transient resonance Raman spectroscopy data obtained in the highly similar truncated HbO from Mycobacterium tuberculosis [29]. Both HbO and HbN do not show microsecond or even nanosecond relaxation of the photoproducts obtained with an 8 ns laser pulse. Hence, the iron histidine stretching frequencies of the deoxygenated species and that of the 10 ns photoproduct are identical pointing to the absence of a proximal strain in truncated hemoglobins [29]. The presence of band III at 772 nm in Tf-trHb is in line with the observations reported for HbO and provides further evidence that the structure of the proximal site in the static deoxygenated derivative in truncated hemoglobins may be similar to the structure of the transient, unrelaxed photoproduct species in classical globins. Transient spectroscopy measurements in the near infrared region in Tf-trHb will provide a further proof of this picture.

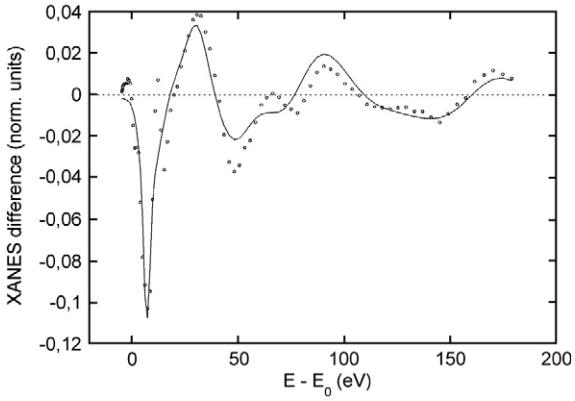

Fig. 4. XANES analysis. Best fit of the XANES difference spectrum [Tf-trHb–h-Mb]. The experimental spectrum is the dotted line while the theoretical curve is the solid one.

The EXAFS and XANES data directly provide a high resolution map of the iron first-shell distances changes with 0.01–0.03 Å accuracy. The measurements, carried out in parallel on the deoxygenated derivatives of h-Mb and Tf-trHb bring out major differences between the two proteins that are manifest in the FT spectrum shown in Fig. 2. Quantitative analysis, reported in Tables 1 and 2, points out two major features of the Fe-proximal histidine environment in Tf-trHb. First of all, the calculated Fe–N_h distance in Tf-trHb is unusually short (1.90 Å) with respect to that of h-Mb (2.14 Å). The 0.24 Å difference in the bond length between the two proteins represents a dramatic difference in terms of bond orbital energy and points to an optimal overlap between the iron and N_h orbitals as a consequence of a fully relaxed position of the imidazole ring [26]. The second important structural feature concerns the average out-of-plane position of the iron atom with respect to the heme plane as inferred from the calculated Fe–pyrrole nitrogen distances. In this case, the positioning of the iron atom relative to the pyrrole nitrogens is identical in h-Mb and Tf-trHb (average distances of 2.06 Å in h-Mb, 2.05 Å in Tf-trHb) pointing out that the heme core size must be superimposable in the two proteins. Thus, the differences in the EXAFS and XANES spectra between h-Mb and Tf-trHb are entirely accounted for a shorter Fe–N_h bond distance with minimal, if any, readjustments of the heme core size. In turn, in agreement with X-ray crystallographic data on the ferric, acetate bound adduct, the stronger Fe–N_h bond in Tf-trHb indicates an unrestrained conformation of the proximal histidine. Nevertheless, it should be mentioned that red shifted band III derivatives can also be generated at equilibrium by acting on solvent properties [30]. High glycerol concentrations or sol–gel encapsulation are capable of shifting the peak position of band III towards the blue region by promoting dehydration of the protein. The ultimate effect of the removal of protein coordinated water may thus be ascribed to local collapse of the heme pocket with subsequent fine structural rearrangements of the heme-iron position.

Hence, in structural terms, the position of band III reflects the fine structural modifications within the iron atom coordination sphere in response to chemical and physical perturbations. Although the present data offer a unique opportunity to correlate the iron coordinates (as measured in EXAFS experiments) with the position of band III, another possible explanation can be envisaged. In fact, a possible interpretation would be a direct relationship between the Fe–N_h distance and the frequency of the electronic transition, assuming that the energy of the porphyrin π system is superimposable in Tf-trHb and h-Mb. However,

inspection of the visible spectra suggests that the overall electronic structure of the porphyrin π system is not superimposable. In fact, in Tf-trHb, the peak position of the deoxygenated derivative is at 432 nm and hence red shifted with respect to h-Mb (435 nm) [16]. The Soret peak energies are affected by the overall electron density of the heme thus suggesting that there is a small but significant electron withdrawing effect (which enhances the energy of the $\pi \rightarrow \pi^*$ transitions), in Tf-trHb with respect to h-Mb. It has been proposed that there are at least two different mechanisms that may promote π electron withdrawal/donation from/to the porphyrin ring, namely: i) increased hydrogen bonding to N_δ of the proximal ligand that promotes electron donation from Fe–N_h via the proximal imidazole ring and shortens the iron histidine bond distance, and ii) increased conjugation of the vinyl double bonds with the porphyrin π system that favors electron donation and lowers the $\pi \rightarrow \pi^*$ transition energies [31]. In the case of Tf-trHb, the observed blue shift of the Soret band, due to decreased π electron density, might be ascribed mainly to the short iron histidine bond but in the absence of concomitant hydrogen bonding donation to the N_δ of the proximal ligand (see also next paragraph) and hence without the "electron push" effect. In turn, the effect of vinyl conjugation still needs to be investigated in detail by appropriate resonance Raman experiments, although no major "out-of-plane" shift of the double bonds is evident from inspection of the available X-ray structure [16]. In summary, the inverse relationship between the red shifted band III and blue shifted Soret spectrum in Tf-trHb might find a rationale in terms of electronic configuration only assuming an electron withdrawal effect by the proximal imidazole ring, fully protonated at the N_δ.

These considerations pave the way to a broader discussion on the architecture of the proximal site with respect to different heme proteins other than globins. First of all, it is of interest to describe the environment of the proximal histidine in Tf-trHb in structural terms, by taking into account that the only available X-ray structure (2BMM in the PDB databank) concerns the ferric, acetate bound derivative. In Tf-trHb, the imidazole ring of His106(F8) is comprised between residues Tyr109, Met151 and the peptide bond of Leu111 (see Fig. 5A). None of these residues appear to interact directly with HisF8 but they simply delimit an apolar cavity in which the imidazole ring is almost rotamerically free with the exception of a small angle in which the sulphur atom of Met151 hinders full rotation. Accordingly, by inspecting the position of the imidazole plane with respect to the porphyrin nitrogen plane (Fig. 5B), it is apparent that the imidazole plane itself is in a fully staggered (with respect to N_p pyrrole atoms) and hence relaxed position. Thus, it might be suggested that the overall architecture of the proximal site in Tf-trHb is such that the iron–histidine bond is free of constraint and is able to reach maximal bonding overlap. Several studies in past years have revealed consistent differences between the structure of the heme in globins and peroxidases [31]. As shown from XAS and high resolution X-ray structures, globins typically have an Fe–N_h distance of about 2.1 Å while in the peroxidases this distance is typically shorter by about 0.2 Å, resulting in a typical Fe–N_h distance of about 1.9 Å [31–38] (see also Table 3). This was proposed to be crucial to explain the different reactivity observed between the two groups of proteins [34,35]. A significant feature of the peroxidase structures (either Cytochrome *C* peroxidase, Ccp, or Horseradish peroxidase, Hrp) is the presence of strongly hydrogen-bonding proximal histidine [38]. In CcP, the side-chain carboxylate of Asp235 is H-bonded to both Trp191 and His175, the proximal ligand of the heme-iron. The strong H-bond is believed to result in increased electron density on the porphyrin system, which would aid in stabilizing the heme and radical centers in the transition complex. The globins, typified by h-Mb, lack this strong hydrogen bonding to the proximal histidine and exhibit a longer Fe–N_h bond. Moreover, the orientation of the imidazole plane with respect to the pyrrole nitrogen plane is such that the proximal histidine is in a fully eclipsed rotameric conformation that precludes optimal overlap of the iron axial and histidine nitrogen orbitals [36,37].

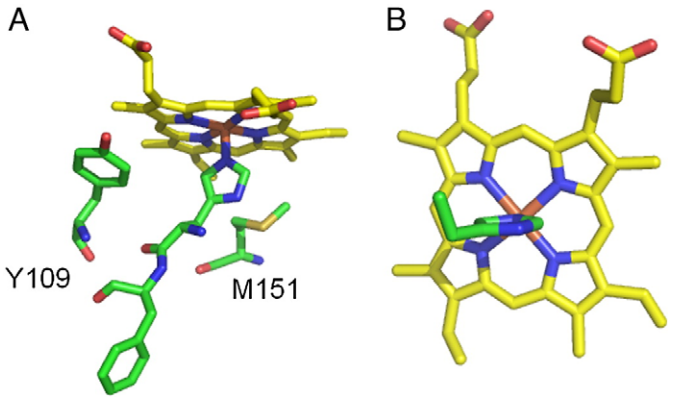

Fig. 5. Close up view of the proximal site in Tf-trHb. The X-ray structure (2BMM) of ferric Tf-trHb is characterized by a triad of aminoacids surrounding the proximal histidine (A). The plane of the imidazole ring lies perpendicular and in a fully staggered position with respect to the four pyrrole nitrogen (B).

In conclusion, the picture that emerges from the comparison of proximal sites among Tf-trHb, typical globins and heme peroxidases is that a combination of proximal effects may be responsible for the tuning of the iron histidine bond distance which in turn is a key determinant for the heme reactivity. In this framework, the unique architecture of the Tf-trHb proximal site lies in between globin and peroxidases. The short iron–histidine distance implies a peroxidase-like environment that suggests a catalytic role towards hydrogen peroxide in truncated hemoglobins. As a matter of fact, a robust peroxidase-like activity has been recently demonstrated in Tf-trHb and in the highly similar truncated globin from *Mycobacterium tuberculosis* [39,40]. In turn, in Tf-trHb, the short iron–histidine bond is not the consequence of a strong hydrogen bonding to the N_δ of the imidazole ring, as is commonly observed in genuine peroxidases. Thus, from the point of view of the proximal site properties, Tf-trHb can be considered as a hybrid between a globin and a peroxidase whereas its biochemical function most likely corresponds to that of the latter protein.

Acknowledgment

Financial support by the Italian Ministry of University and Research [Linea D1 "ex-60%" 2007–2008 Università Cattolica Sacro Cuore] is gratefully acknowledged. This work was also supported by CASPUR with the Standard HPC Grant 2009 entitled: "A combined X-ray absorption spectroscopy, Molecular Dynamics simulations and Quantum Mechanics calculation procedure for the structural characterization of ill-defined systems". We acknowledge the European Synchrotron Radiation Facility for provision of synchrotron radiation facilities and the staff of BM30B for the helpful support. We are grateful to Stefano Della Longa for many helpful discussions. Project from Fondazione Cenci Bolognetti to A.B. is also gratefully acknowledged.

Table 3
Fe–N_h distance in different globins and peroxidases as determined by XAS and XRD.

Protein	Fe–N_h (Å)
Dehaloperoxidase [43]	2.18
Sperm whale myoglobin [37]	2.14
Scapharca hemoglobin [41]	2.19
Human hemoglobin [42]	2.16/2.2
Lignin peroxidase H2 [33]	1.93
Cytochrome *C* peroxidase [34]	1.90

References

[1] M.F. Perutz, Stereochemistry of cooperative effects in hemoglobin. Bohr effect and combination with organic phosphates, Nature 228 (1970) 726–739.
[2] M.F. Perutz, A.J. Wilkinson, M. Paoli, G.G. Dodson, The stereochemical mechanism of the cooperative effects in hemoglobin revisited, Annu. Rev. Biophys. Biomol. Struct. 27 (1998) 1–34.
[3] J.M. Friedman, D.L. Rousseau, M.R. Ondrias, R.A. Stepnoski, Transient Raman study of hemoglobin: structural dependence of the iron-histidine linkage, Science 218 (1982) 1244–1246.
[4] T.W. Scott, J.M. Friedman, Tertiary-structure relaxation in hemoglobin: a transient Raman study, J. Am. Chem. Soc. 106 (1984) 5677–5687.
[5] W.A. Eaton, J. Hofrichter, Polarized absorption and linear dichroism spectroscopy of hemoglobin, Methods Enzymol. 76 (1981) 175–261.
[6] M.W. Makinen, A.K. Churg, Iron Porphyrin Part 1 B, in: B.P. Lever, H.B. Gray (Eds.), Addison Wesly, Reading, MA, 1983, pp. 141–235.
[7] M. Chavez, H. Courtney, M. Chance, D. Kiula, J. Nocek, B. Hofinan, J.M. Friedman, M. Ondrias, Structural and functional significance of inhomogeneous line broadening of band III in hemoglobin and [iron–manganese] hybrid hemoglobins, Biochemistry 29 (1990) 4844–4852.
[8] S. Della Longa, M. Benfatto, Probing the coordination and geometry of heme-iron ligands in hemoproteins by XANES (X-ray absorption near edge structure), Recent Res. Dev. Proteins 1 (2002) 317–343.
[9] A. Filipponi, A. Di Cicco, C.R. Natoli, X-ray-absorption spectroscopy and n-body distribution functions in condensed matter. I. Theory, Phys. Rev. B 52 (1995) 15122–15134.
[10] M. Benfatto, S. Della Longa, Geometrical fitting of experimental XANES spectra by a full multiple-scattering procedure, J. Synchrotron Radiat. 8 (2001) 1087–1094.
[11] S. Della Longa, A. Arcovito, M. Benfatto, A. Congiu-Castellano, M. Girasole, J.L. Hazemann, A. Lo Bosco, Redox-induced structural dynamics of Fe-heme ligand in myoglobin by X-ray absorption spectroscopy, Biophys. J. 85 (2003) 549–558.
[12] P. D'Angelo, M. Benfatto, S. Della Longa, N.V. Pavel, Combined XANES and EXAFS analysis of Co^{2+}, Ni^{2+}, and Zn^{2+} aqueous solutions, Phys. Rev. B 66 (2002) 064209-7.
[13] P. D'Angelo, D. Lucarelli, S. Della Longa, M. Benfatto, J.L. Hazemann, A. Feis, G. Smulevich, A. Ilari, A. Bonamore, A. Boffi, Unusual heme iron-lipid acyl chain coordination in Escherichia coli flavohemoglobin, Biophys. J. 86 (2004) 3882–3892.
[14] P. D'Angelo, A. Lapi, V. Migliorati, A. Arcovito, M. Benfatto, O.M. Roscioni, W. Meyer-Klaucke, S. Della Longa, X-ray absorption spectroscopy of hemes and hemeproteins in solution: multiple scattering analysis, Inorg. Chem. 46 (2008) 7742–7748.
[15] A. Arcovito, T. Moschetti, P. D'Angelo, G. Mancini, G.B. Vallone, M. Brunori, S. Della Longa, An X-ray diffraction and X-ray absorption spectroscopy joint study of neuroglobin, Arch. Biochem. Biophys. 475 (2008) 7–13.
[16] A. Bonamore, A. Ilari, L. Giangiacomo, A. Bellelli, V. Morea, A. Boffi, A novel thermostable hemoglobin from the actinobacterium Thermobifida fusca, FEBS J. 272 (2005) 4189–4201.
[17] O. Proux, X. Biquard, E. Lahera, J.J. Menthonnex, A. Prat, O. Ulrich, Y. Soldo, P. Trevisson, G. Kapoujyan, G. Perroux, P. Taunier, D. Grand, P. Jeantet, M. Deleglise, J.P. Roux, J.L. Hazemann, FAME: a new beamline for X-ray absorption investigations of very-diluted systems of environmental, material and biological interests, Phys. Scr. T115 (2005) 970–973.
[18] O. Proux, V. Nassif, A. Prat, O. Ulrich, E. Lahera, X. Biquard, J.J. Menthonnex, J.L. Hazemann, Feedback system of a liquid-nitrogen-cooled double-crystal monochromator: design and performances, J. Synchrotron Radiat. 13 (2006) 59–68.
[19] A. Filipponi, A. Di Cicco, X-ray-absorption spectroscopy and n-body distribution functions in condensed matter. II. Data analysis and applications, Phys. Rev. B 52 (1995) 15135–15149.
[20] H.H. Zhang, A. Filipponi, A. Di Cicco, M.J. Scott, R.H. Holm, B. Hedman, K.O. Hodgson, Multiple-edge XAS studies of cyanide-bridged iron-copper molecular assemblies relevant to cyanide-inhibited heme-copper oxidases using four-body multiple-scattering analysis, J. Am. Chem. Soc. 119 (1997) 2470–2476.
[21] A. Arcovito, D.C. Lamb, G.U. Nienhaus, J.L. Hazemann, M. Benfatto, S. Della Longa, Light-induced relaxation of photolyzed carbonmonoxy myoglobin: a temperature-dependent X-ray absorption near-edge structure (XANES) study, Biophys. J. 88 (2005) 2954–2964.
[22] S. Della Longa, A. Arcovito, M. Girasole, J.L. Hazemann, M. Benfatto, Quantitative analysis of X-ray absorption near edge structure data by a full multiple scattering procedure: the Fe–CO geometry in photolyzed carbonmonoxy-myoglobin single crystal, Phys. Rev. Lett. 87 (2001) 155501–155504.
[23] A. Labhardt, C. Yven, X-ray absorption edge fine structure spectroscopy of the active site heme of cytochrome *c*, Nature 277 (1979) 150–151.
[24] S. Della Longa, A. Arcovito, B. Vallone, A. Congiu Castellano, R. Kahn, J. Vicat, Y. Soldo, J.L. Hazemann, Polarized X-ray absorption spectroscopy of the low-temperature photoproduct of carbonmonoxy-myoglobin, J. Synchrotron Radiat. 6 (1999) 1138–1147.
[25] S. Pin, B. Alpert, A. Congiu-Castellano, S. Della Longa, A. Bianconi, X-ray absorption spectroscopy of hemoglobin, Methods Enzymol. 232 (1994) 266–292.
[26] M.K. Ellison, C.E. Schultz, W.R. Scheidt, Structure of the deoxymyoglobin model [Fe(TPP)(2-MeHIm)] reveals unusual porphyrin core distortions, Inorg. Chem. 41 (2002) 2173–2181.
[27] M. Sassaroli, D.L. Rousseau, Time dependence of near-infrared spectra of photodissociated hemoglobin and myoglobin, Biochemisty 30 (1987) 3092–3097.
[28] L. Cordone, A. Cupane, M. Leone, E. Vitrano, Thermal behavior of the 760-nm absorption band in photodissociated sperm whale carbonmonoxymyoglobin at cryogenic temperature: dependence on external medium, Biopolymers 27 (1990) 1977–1997.
[29] U. Samuni, Y. Ouellet, M. Guertin, J.M. Friedman, S.R. Yeh, The absence of proximal strain in the truncated hemoglobins from Mycobacterium tuberculosis, J. Am. Chem. Soc. 126 (2004) 2682–2683.
[30] J. Huang, M. Leone, A. Boffi, J.M. Friedmann, E. Chiancone, Near-infrared spectra of Scapharca homodimeric hemoglobin: characterization of the deoxy and photodissociated derivatives, Biophys. J. 70 (1996) 2924–2929.
[31] L. Powers, Molecular Electronics and Molecular Electronic Devices, Vol. 3, pp 211–222, CRC Press Inc., Boca Raton, FL, 1994.
[32] B. Chance, L. Powers, Y. Ching, T. Poulos, G.R. Schonbaum, Y. Yamazaki, G.K. Paul, X-ray absorption studies of intermediates in peroxidase activity, Arch. Biochem. Biophys. 235 (1984) 596–611.
[33] R. Sinclair, I. Yamazaki, J. Bumpus, B. Brock, C.S. Chang, A. Albo, L. Powers, Structure of the active site of lignin peroxidase isozyme H2: native enzyme, compound III, and reduced form, Biochemistry 31 (1992) 4892–4900.
[34] R. Sinclair, S. Hallam, M. Chen, B. Chance, L. Powers, Active site structure in cytochrome *c* peroxidase and myoglobin mutants: effects of altered hydrogen bonding to the proximal histidine, Biochemistry 35 (1996) 15120–15128.
[35] M. Chance, L. Parkhurst, L. Powers, B. Chance, Movement of Fe with respect to the heme plane in the R–T transition of carp hemoglobin. An extended x-ray absorption fine structure study, J. Biol. Chem. 261 (1986) 5689–5692.
[36] F. Yang, G.N. Phillips Jr., Crystal structures of CO-, deoxy- and met-myoglobins at various pH values, J. Mol. Biol. 256 (1996) 762–774.
[37] C. Lionetti, M.G. Guanziroli, F. Frigerio, P. Ascenzi, M. Bolognesi, X-ray crystal structure of the ferric sperm whale myoglobin: imidazole complex at 2.0 A resolution, J. Mol. Biol. 217 (1991) 409–412.
[38] J. Peisach, An interim report on electronic control of oxygenation of heme proteins, Ann. N.Y. Acad. Sci. 244 (1975) 187–200.
[39] H. Ouellet, K. Ranguelova, M. Labarre, J.B. Wittenberg, B.A. Wittenberg, R.S. Magliozzo, M. Guertin, Reaction of Mycobacterium tuberculosis truncated hemoglobin O with hydrogen peroxide: evidence for peroxidatic activity and formation of protein-based radicals, J. Biol. Chem. 282 (2007) 7491–7503.
[40] R. Torge, A. Comandini, B. Catacchio, A. Bonamore, B. Botta, A. Boffi, Peroxidase-like activity of Thermobifida fusca hemoglobin: the oxidation of dibenzylbutanolide, J. Mol. Catal B: Enzym. 61 (2009) 303–308.
[41] W.E. Royer Jr, High-resolution crystallographic analysis of a co-operative dimeric hemoglobin, J. Mol. Biol. 235 (1994) 657–681.
[42] S.Y. Park, T. Yokoyama, N. Shibayama, Y. Shiro, J.R. Tame, 1.25 A resolution crystal structures of human haemoglobin in the oxy, deoxy and carbonmonoxy forms, J. Mol. Biol. 360 (2006) 690–701.
[43] Z. Chen, V. de Serrano, L. Betts, S. Franzen, Distal histidine conformational flexibility in dehaloperoxidase from Amphitrite ornata, Acta Crystallogr. D Biol. Crystallogr. 65 (2009) 34–40.